Finite element modeling of high-pressure deformation and phase transformation of silicon beneath a sharp indenter

2009 Semicond. Sci. Technol. 24 025014

(http://iopscience.iop.org/0268-1242/24/2/025014)

Semicond. Sci. Technol. **25** (2009) 025014 (12pp) doi:10.1088/0268-1242/25/2/025014

Finite element modeling of high-pressure deformation and phase transformation of silicon beneath a sharp indenter

Tadao Kiriyama[1], **Hirofumi Harada**[2] **and Jiwang Yan**[3,4]

[1] Nippon Steel Materials Co., Ltd, 2-6-3 Otemachi, Chiyoda-ku, Tokyo 100-8071, Japan
[2] Siltronic Japan Corporation, 3434 Shimata, Hikari, Yamaguchi 743-0063, Japan
[3] Department of Nanomechanics, School of Engineering, Tohoku University, Aramaki Aoba 6-6-01, Aoba-ku, Sendai, 980-8579, Japan

E-mail: yanjw@pm.mech.tohoku.ac.jp

Received 10 September 2008, in final form 10 November 2008
Published 9 January 2009
Online at stacks.iop.org/SST/25/025014

Abstract

Modeling of the mechanical response of single crystalline silicon to a sharp indenter is an essential step for the optimization of wafer manufacturing processes. In this paper, deformation of silicon during indenter loading and unloading was analyzed by the finite element method, and the changes of stress field and high-pressure phase distribution were dynamically simulated. We found that the deformation of silicon in nanoindentation can be simply characterized by two factors: one is the elastic strain of each high-pressure phase and the other is the equivalent elastic strain of each phase transformation. In loading, indentation energy is absorbed mostly by phase transformation, and accumulated as the elastic strain of the high-pressure phases. The distribution pattern of the high-pressure phases beneath the indenter is independent of the indentation load, and the depth of the phase-transformed region is approximately twice the indentation depth. In unloading, high-pressure phases except the β-Sn phase undergo reverse phase transformations. The β-Sn phase does not transform back to the diamond phase but changes to other non-equilibrium phases, which becomes the dominant reason for residual strain. During unloading, the non-equilibrium phase expands from the diamond phase region toward the indenter tip, while the boundary between the non-equilibrium phase and the diamond phase remains unchanged. The unloading mechanism is independent of the change in the maximum indentation load and the presence/absence of pop-out events.

(Some figures in this article are in colour only in the electronic version)

1. Introduction

Single-crystal silicon is not only an important semiconductor substrate material, but also an excellent infrared optical material. Precision manufacturing (slicing, grinding, lapping, polishing and cutting) technology of large-diameter silicon wafers has become one of the important research focuses of the microelectronic, micromechanical and optical manufacturing industries. To date, there have already been a lot of experimental studies on the micro machining mechanism and subsurface damage of silicon [1–7].

Nanoindentation is an effective method to investigate the machining mechanism and the subsurface damage of a material, i.e., the responses of the material to tools (including single point cutting tools and multipoint abrasive tools) in terms of brittle fracture, plastic deformation and microstructural change. Phase transformation and dislocation motion are two possible reasons for silicon deformation. An abundance of literature has demonstrated that in nanoindentation, silicon undergoes phase transformation [8–19]. It is generally accepted that during loading a structural change from a diamond cubic state into a metallic state β-Sn occurs under the indenter due to the high pressure (10–13 GPa). Material around the indenter would then become sufficiently

[4] Corresponding author.

ductile to sustain plastic flow. In unloading, the metallic phase does not transform back to the diamond cubic structure, but instead, changes to an amorphous phase or other metastable phases. The residual indent depth increases with the maximum indentation load, and pop-out events sometimes occur in the load–displacement curves. These findings in nanoindentation studies are essentially helpful to understand the micro/nano machining mechanism of silicon.

Phase transformation of silicon is very sensitive to pressure. It has been known from high-pressure diamond anvil tests that as the pressure increases, the structure of silicon changes sequentially from the diamond phase to the β-Sn phase, the primitive hexagonal (PrimHex) phase and the close packed hexagonal (HCP) phase. In a nanoindentation test, since the stress state in the material beneath the indenter is strongly time and location dependent, the high-pressure phase distribution of silicon is a very complicated issue. However, to date, there is no available literature focused on the dynamic changes in the distributions of stress/strain and high-pressure phases in the nanoindentation process of silicon. For the fact that the high-pressure phases cannot be directly *in situ* observed during nanoindentation by experimental methods, such as transmission electron microscopes (TEM), simulation by the finite element method (FEM) may be an effective approach to investigate this issue.

Conventionally, in the FEM simulation of the indentation of metal materials where no high-pressure phase transformation occurs, elastic/plastic deformation is incorporated into the material property definition as a function of strain. For silicon, Yoshino *et al* [20] used the *fcc* lattice structure to approximate the diamond structure and they dealt with the phase transformation from the diamond phase to the β-Sn phase as shear deformation of the *fcc* lattice in their nanoindentation simulation. According to their model, the residual defects of silicon are a kind of slip deformation caused by the shear stress during loading. Hebbache *et al* [21] investigated the phase transformation from the diamond structure to the β-Sn phase based on shear stress analysis, but did not consider other phase transformations at much higher pressure levels. As a recent progress, Vondenitcharova and Zhang [22] conducted the FEM analysis of silicon indentation by considering phase transformations. They preset a yielding condition to diamond-phase silicon. As a result, an elastic/plastic boundary is generated in silicon after loading. They approximated the phase transformations of silicon from the low-pressure phases to the PrimHex phase and the HCP phase, which occur at much higher pressures than that of the β-Sn phase, to plastic deformation phenomena, and used the average mechanical property (bulk modulus) of these high-pressure phases in their simulation.

However, the approximation of high-pressure phase transformation to plastic deformation might be an inaccurate approach. As known from most of the available literature on the indentation tests of silicon, dislocation-based plastic deformation is by far insignificant in comparison with phase transformation. It is the phase transformation that releases the externally applied stresses. In other words, the high pressure causes silicon to change into a denser structure with a smaller lattice constant, and in turn, a decrease in the material volume. As the applied stress is beyond the critical stress/pressure, phase transformation takes place instantaneously without the need for any other activation. Then, as the stress/pressure increases further, the volume of the high-pressure phase decreases through elastic deformation.

In the present study, we conducted the FEM simulation of silicon nanoindentation to visualize the changes in the distribution of stress and high-pressure phases beneath a sharp indenter during the loading and unloading processes. We modeled the material property of silicon via a new approach. To precisely describe the mechanical property changes of silicon, we dealt with each high-pressure phase (diamond phase, β-Sn phase, PrimHex phase and HCP phase) and the transformations among these phases individually by considering the dynamic change of the stress field in the indented zone. Instead of approximating the phase transformations to plastic deformations, we treated them as equivalent elastic deformations and used two factors to describe the property of silicon: one is the elastic modulus (Young's modulus) for each high-pressure phase, and the other is the equivalent elastic modulus for the strain relaxed by phase transformations. By fitting the simulated load–displacement curves to the experimental results, we established the mechanical characteristics of all the high-pressure phases and the phase transformations. We will also demonstrate that the strain energy accumulated during loading will be converted into residual strain of the non-equilibrium phases generated in nonreversible phase transformation during unloading. In addition, the relationships among the residual strain, the distribution of the non-equilibrium silicon phases and the indentation load will be investigated. The results from this study will be helpful to clarify the deformation mechanism and the subsurface damage mechanism of silicon in the mechanical contacts and wafer manufacturing processes.

2. Nanoindentation experiments

To verify the FEM models proposed in this study and compare with the simulated results, nanoindentation tests were performed using a nanoindentation tester, ENT-1100a, produced by Elionix Co. Ltd, Japan. Tests were performed using a Berkovich indenter made of single-crystal diamond. Usually, a Berkovich indenter can be considered as completely sharp. However, due to technological limitations, the indenter cannot be absolutely sharpened and will inevitably have a radius (ranging from a few tens of nanometers to a few hundreds of nanometers). When the indentation depth is big, the influence of the tip radius is so small that the indenter can be considered as a sharp one. However, when the indentation depth is small, the effect of the tip radius cannot be neglected. In this paper, to guarantee the data accuracy and reliability, we experimentally measured the tip radius of the indenter, and used the same tip radius value in FEM simulation. The indenter tip was measured by a special scanning electron microscope (SEM) equipped with two electron detectors. Figure 1 shows a three-dimensional topography of the indenter tip, from which the tip radius was estimated to be approximately 200 nm.

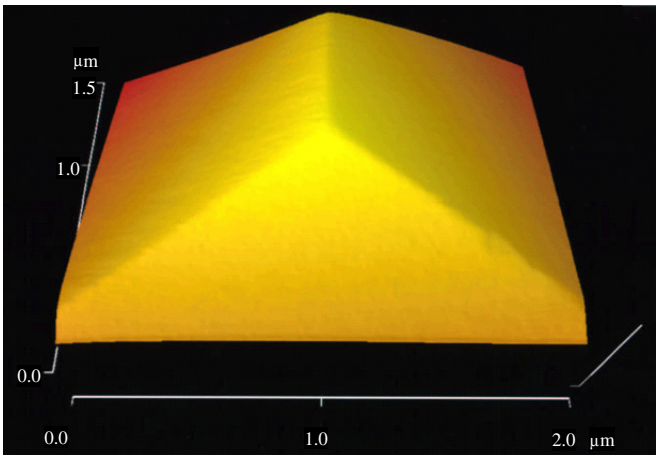

Figure 1. Three-dimensional topography of the diamond-indenter tip measured by a special scanning electron microscope.

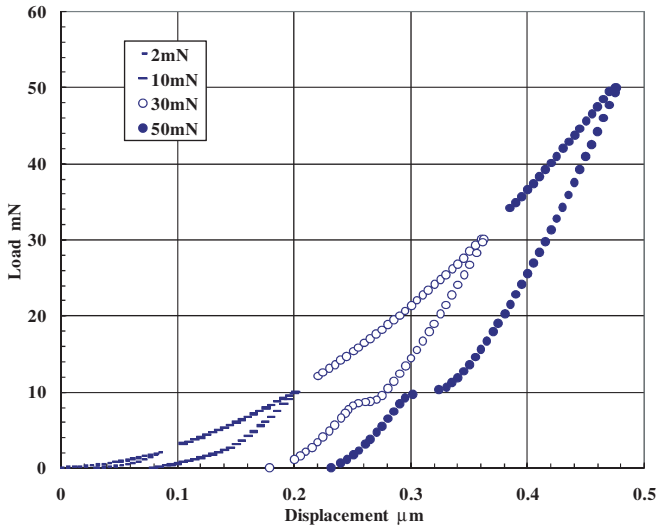

Figure 2. Typical nanoindentation load–displacement curves at various maximum loads.

The maximum load was varied in the range of 2–50 mN and the time for loading and unloading was fixed to 5 s; thus, the loading/unloading rate changed in the range of 0.4–10 mN s^{-1}.

A p-type single-crystal silicon wafer having a doping level of 1.33 × 10^{14} atoms cm^{-3} was used as a specimen. The surface orientation of the silicon wafer is (0 0 1). The wafer is 0.725 mm in thickness and obtained with chemo-mechanical polished finish. The orientation flat [1 1 0] of the silicon wafer was adjusted to be parallel to one face of the indenter. After indentation tests, cross-sectional TEM observations of the indents were performed. It was found that the material just under the indenter has been transformed into a non-equilibrium silicon phase (amorphous phase dotted by microcrystalline grains), and dislocations were very few. The observation results were similar to those in [19].

Figure 2 shows typical load–displacement curves during the indentations at various maximum loads: 2, 10, 30 and 50 mN. It can be seen that the maximum displacement of the indenter and the residual depth of the indents both increase

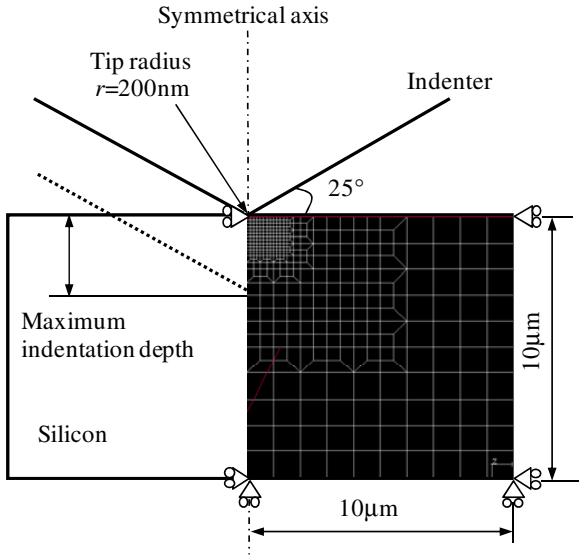

Figure 3. Two-dimensional axisymmetrical model for FEM simulation.

with the maximum indentation load. However, the four curves are identical following the same trend in the loading stage despite the difference in the maximum load. This fact indicates that the deformation mechanism of silicon during loading is independent of the indentation load. From figure 2, it can be seen that at the maximum loads of 30 and 50 mN, the unloading curves show apparent pop-out events at a load of about 10 mN, while when the maximum loads are 2 mN and 10 mN, no pop-out occurs.

3. FEM model

FEM simulation was performed using a commercially available finite element program, Mark-Mentat, produced by MSC Co. Ltd. For simplicity, we used a two-dimensional axisymmetrical model as shown in figure 3. In the model, the width and the height of the silicon material were both set to 10 μm. To minimize calculation time, we used a smaller mesh size of 0.25 μm for the material around the indenter tip where the deformation is the most intensive, and used larger mesh size for the surrounding area. In total, 400 elements were used. Automatic remeshing was performed during the calculation for improving the simulation accuracy.

As boundary conditions, the symmetrical axis and the right boundary of the silicon material were fixed in the horizontal direction, and the bottom of the material was fixed in the vertical direction. The diamond indenter was regarded as a completely rigid body without deformation. The friction coefficient between the diamond indenter and silicon material was set to 0.2. The indenter tip radius was set to 200 nm, the same as the experimentally measured value from figure 1. The angle between the side face of the indenter and the silicon surface was set to 25°. Heat generation and the temperature change of the specimen material due to indentation were not considered.

Table 1. Lattice constants and lattice atomic numbers of various silicon phases under different levels of hydrostatic pressures.

Silicon phases	Hydrostatic pressure (GPa)	Lattice constant (Å)		Lattice atomic number	Atomic density (g cm^{-3})	Volumetric change from diamond phase (V/V_0) (%)	References
		a	c				
Diamond		5.431		8	2.329	100	Appendix
β-Sn	11.2	4.69	2.578	4	3.290	70.8	[23]
β-Sn	12.5				3.287	70.9	[24]
β-Sn	10.3	4.665	2.572	4	3.333	69.9	[25]
Primitive hexagonal	16	2.551	2.387	1	3.467	67.2	[23]
Primitive hexagonal	16				3.554	65.5	[27]
Primitive hexagonal	18				3.510	66.4	[24]
Primitive hexagonal	36	2.463	2.32	1	3.826	60.9	[28]
Hexagonal close packed	41	2.524	4.142	2	4.082	57.1	[26]
Hexagonal close packed	43	2.444	4.152	2	4.343	53.6	[27]
Hexagonal close packed	78.3						[29]
BC8	13.4	6.636		16	2.554	91.2	Phase diagram
BC8	10	6.405		16	2.840	82.0	[23, 26]
BC8	1E-4	6.62		16	2.572	90.5	[23, 26]
BC8	1E-4				2.554	91.2	[30]
BC8	1E-4				2.552	91.2	[31]
BC8	1E-4	6.67		16	2.515	92.6	[32]
BC8	1E-4				3.929	59.3	[31]
BC8	2	5.716		16	3.996	58.3	[31]
Amorphous	1E-4				2.844	81.9	Appendix

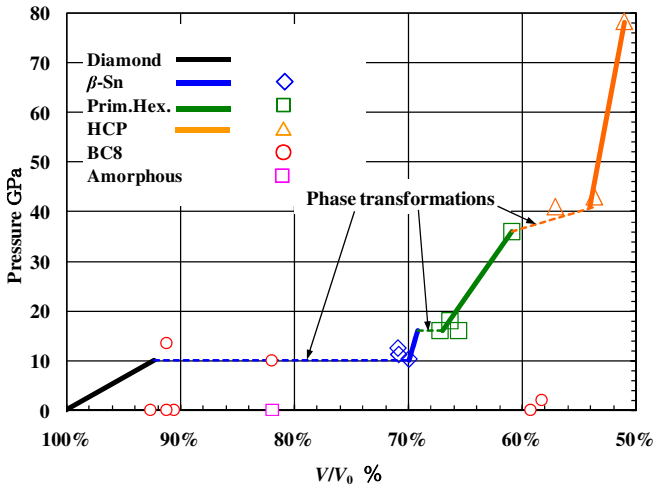

Figure 4. Volumetric changes of the high-pressure phases of silicon plotted with pressure.

4. Stress–strain curves for FEM simulation

4.1. Stress–strain curve for loading

Table 1 lists the previously reported lattice constants and lattice atomic numbers of various silicon phases under different levels of hydrostatic pressures [23–32]. Based on the lattice constants, in the appendix, we calculated the atomic density of each phase and the volumetric changes from the diamond phase to the high-pressure phases (V/V_0). Figure 4 shows a plot of the volumetric change V/V_0 listed in table 1 against pressure. The solid lines show the volume changes due to the elastic deformation of each silicon phase, and the dotted lines indicate the volume changes due to phase transformations. In the figure, it is shown that the circles indicating the data for the BC8 phase show significant dispersion. This is because of the fact that as a non-equilibrium phase, the BC8 phase exists during the unloading process from the high-pressure state, the measurement results of which are strongly dependent on the unloading conditions. From the slopes of the straight lines in figure 4, we calculated the bulk modulus K for each phase of silicon. Then, based on the bulk modulus, we obtained Young's modulus E in single-axis tension which is necessary for FEM simulation. The relationship between Young's modulus and bulk modulus can be described as

$$E = 3K(1 - 2\nu) \tag{1}$$

where ν is Poisson's ratio. In this paper, we fixed ν to 0.279 which is Poisson's ratio of Si (1 1 1), and did not consider the anisotropy in material property. Then, equation (1) becomes

$$E = 1.326K. \tag{2}$$

From equation (2), we obtained the relationship between the strain in single-axis tension $\Delta l/l$ and the volume change $\Delta V/V$ as follows:

$$\frac{\Delta l}{l} = 0.754\frac{\Delta V}{V}. \tag{3}$$

Using the relationship in equation (3) and the data in figure 4, the relationship between stress and strain in single-axis tension of silicon can be obtained as shown in figure 5. This stress–strain curve is adopted in the subsequent FEM simulations of the present study to describe the elastic deformation and phase transformation of silicon during loading.

Table 2 lists the ranges of stress and strain, the average Young's modulus E_{ave}, and the linear approximation equations of Young's modulus E of each silicon phase used in the FEM simulation. For the diamond phase, the elastic deformation is in the range of 0–6% under a stress of 0–10 GPa, and the average Young's modulus in the elastic deformation is

Table 2. Stress, strain, average Young's modulus and linear approximation equations of Young's modulus for the high-pressure phases of silicon.

Si phases	Phase transformations	Stress (GPa)	Strain (%)	E_{ave} (GPa)	Linear approximation equation of E
Diamond		0–10	0–6	163	$E = 11.77 \times (\text{strain}\%) + 127$
	From diamond to β-Sn		6–22	0.163	$E = 0.163$
β-Sn		10–16	22–24	304	$E = 18.35 \times (\text{strain}\%) - 114$
	From β-Sn to PrimHex		24–25	0.163	$E = 0.163$
PrimHex		16–36	25–30	416	$E = 56.34 \times (\text{strain}\%) - 1139$
	From PrimHex to HCP	(36–41)	30–33	163	$E = 163$
HCP		41–	33–	790	$E = 104.36 \times (\text{strain}\%) - 2964$

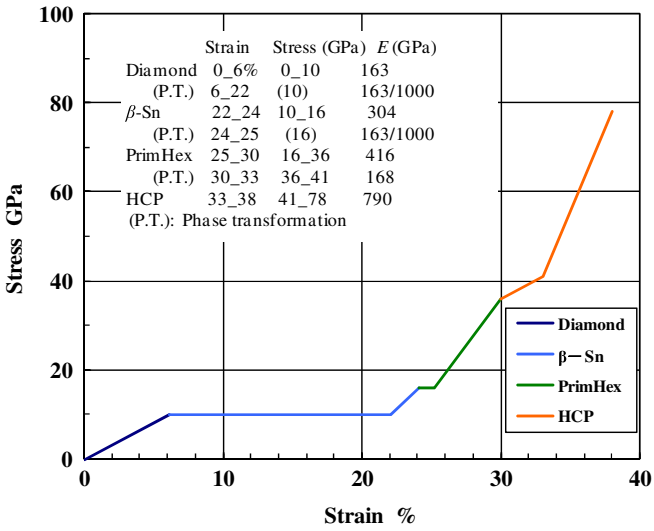

Figure 5. Relationship between stress and strain in the single-axis tension of silicon.

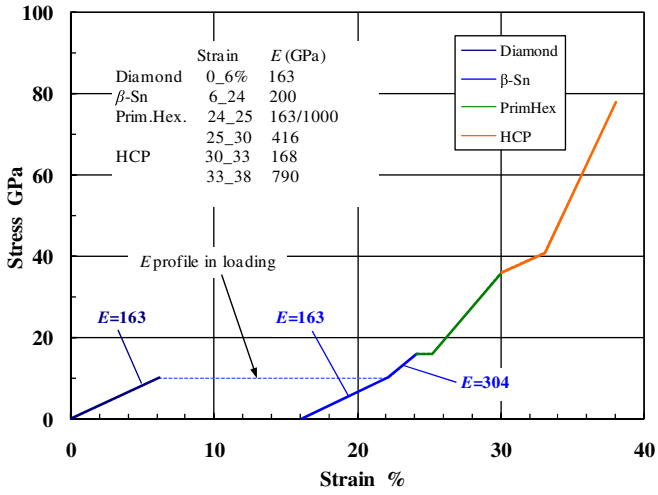

Figure 6. Stress–strain curve used for region 1 (before pop-out) in unloading.

163 GPa. Under a stress of 10 GPa, the diamond phase transforms to the β-Sn phase, the strain relaxation caused by which is 16% (from 6% to 22%). Subsequently, the strain relaxation caused by phase transformation from the β-Sn phase to the PrimHex phase is 1% (from 24% to 25%), and that from the PrimHex phase to the HCP phase is 3% (from 30% to 33%). From these results, we can see that the strain relaxation caused by the phase transformation from the diamond phase to the β-Sn phase is the most significant one. Also, it is evident that Young's modulus of silicon is strongly dependent on the type of high-pressure phase and the value of strain. The higher the strain level, the bigger Young's modulus, and vice versa. This is presumably because, under a higher strain, the interaction force between silicon atoms within the lattice structure becomes stronger. In this work, by individually considering the elastic modulus of each high-pressure phase, the accuracy of the FEM simulation of the silicon indentation process can be improved remarkably.

To incorporate the phase transformation into FEM simulation, we made two assumptions. One assumption is that the volume change due to the phase transformation at the critical stress/pressure is equivalent to an extremely small elastic modulus. The other assumption is that for each silicon phase, the elastic modulus changes linearly. Because the deformation resistance of the transformation from the diamond phase to the β-Sn phase and that from the β-Sn phase to the PrimHex phase are extremely small, we assigned a value of 0.163 GPa (equal to 1/1000 of Young's modulus of the diamond phase) as the equivalent Young's modulus for these two phase transformations. For the transformation from the PrimHex phase to the HCP phase, as there exists a certain degree of deformation resistance, for simplicity, we assigned it an equivalent Young's modulus of 163 GPa, which is the same as that of the diamond phase. The load–displacement curves simulated on the basis of these assumptions were very close to the experimental curves, as shown later in this paper.

4.2. Stress–strain curve for unloading

For the unloading process, if we use the same material properties as those used in the loading process, the unloading curve will coincide with the loading curve and it will be impossible to obtain a residual strain after indentation. Therefore, the material properties of unloading must be different from those of loading. To define the material property, we divided a load–displacement curve of unloading into three regions: the region before pop-out occurrence (region 1), the pop-out region (region 2) and the region after pop-out (region 3).

For region 1, the equivalent Young's modulus of reverse transformation from the β-Sn phase to the diamond phase was set to 163 GPa in the strain range of 6–22%. The equivalent Young's modulus of other phase transformations

Table 3. Material properties used for simulating the unloading process through three regions.

			Young's modulus E (GPa)			
				Unloading		
Si phase	Phase transformation	Strain (%)	Loading	Region 1	Region 2	Region 3
Diamond		0–6	163(∗1)	163[a]	163[a]	163[a]
	From diamond to β-Sn	6–22	0.163	*163*	*16.3*	*163*
β-Sn		22–24	304[b]	304[b]	*16.3*	304[b]
	From β-Sn to PrimHex	24–25	0.163	0.163	*16.3*	0.163
PrimHex		25–30	416[c]	416[c]	*16.3*	416[c]
	From PrimHex to HCP	30–33	163	163	*16.3*	163
HCP		33–	790[d]	790[d]	*16.3*	790[d]

Values in italic font are different from those of the loading process.
[a] Linear approximation equation $E = 11.77 \times (\text{strain}\%) + 127$.
[b] $E = 18.35 \times (\text{strain}\%) - 114$.
[c] $E = 56.34 \times (\text{strain}\%) - 1139$.
[d] $E = 104.36 \times (\text{strain}\%) - 2964$.

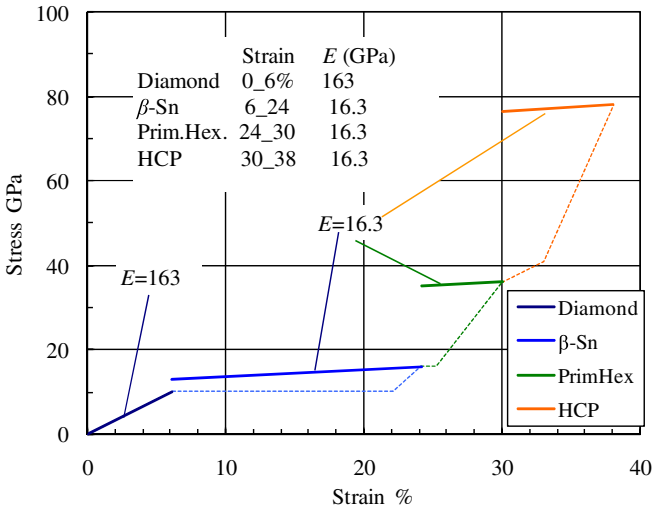

Figure 7. Stress–strain curve used for region 2 (pop-out region) in unloading.

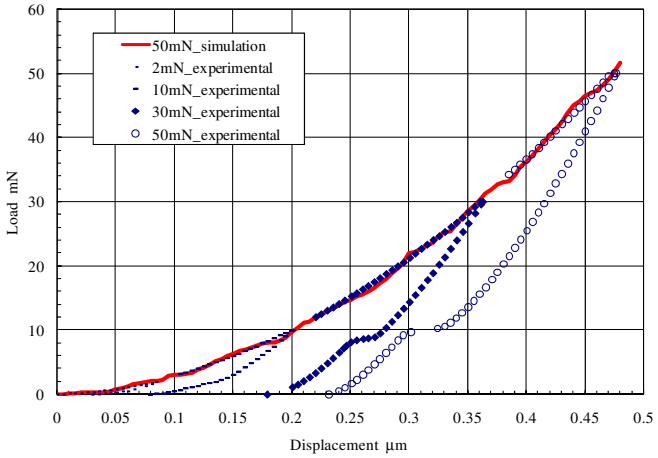

Figure 8. Simulated load–displacement curve at a maximum load of 50 mN together with the experimental data.

and Young's modulus of each silicon phase were the same as those used in loading. The stress–strain curve used for region 1 is shown in figure 6. For region 2, Young's modulus of all the silicon phases (except for the diamond phase) and the equivalent modulus of all phase transformations were set to a small value of 16.3 GPa, equal to 1/10 of that of the diamond phase. The stress–strain curve used for region 2 is shown in figure 7. In region 3, the same stress–strain relationship was used as that of region 1. The material properties for all three regions are listed in table 3. Poisson's ratio for unloading is the same as that used for loading. Using the material property definitions in table 3, the simulated curves were closely fitted to the experimental curves.

5. Results and discussion

5.1. Results of the loading process

5.1.1. Load–displacement curve. On the basis of the stress–strain relationship shown in figure 5 and table 2, the FEM simulation of the loading process was carried out using the FEM model in figure 3. A load–displacement curve simulated during the loading process (maximum load: 50 mN) is plotted in figure 8 by the solid line. The dotted lines are the experimental data. Despite the slight waviness of the simulated curve, which might have been caused by the computational instability, it is evident that the simulated load–displacement curve is in agreement with the experimental data.

5.1.2. Distribution of high-pressure phases. Figure 9 is a simulated distribution of strain in silicon at a load of 50 mN. The scale bar in the figure corresponds to the horizontal axes of figures 5, 6 and 7, where the strain was presented by percentage. The largest strain in figure 9 is over 40%, which occurs just beneath the indenter tip. The strain is a sum of compressive strain and shear strain. According to the strain level, we can presume that the region right beneath the indenter is the HCP phase, around which is the PrimHex phase. The PrimHex phase is further surrounded by the β-Sn phase. The outermost region is diamond-phase silicon. As a result, the high-pressure phases are distributed concentrically

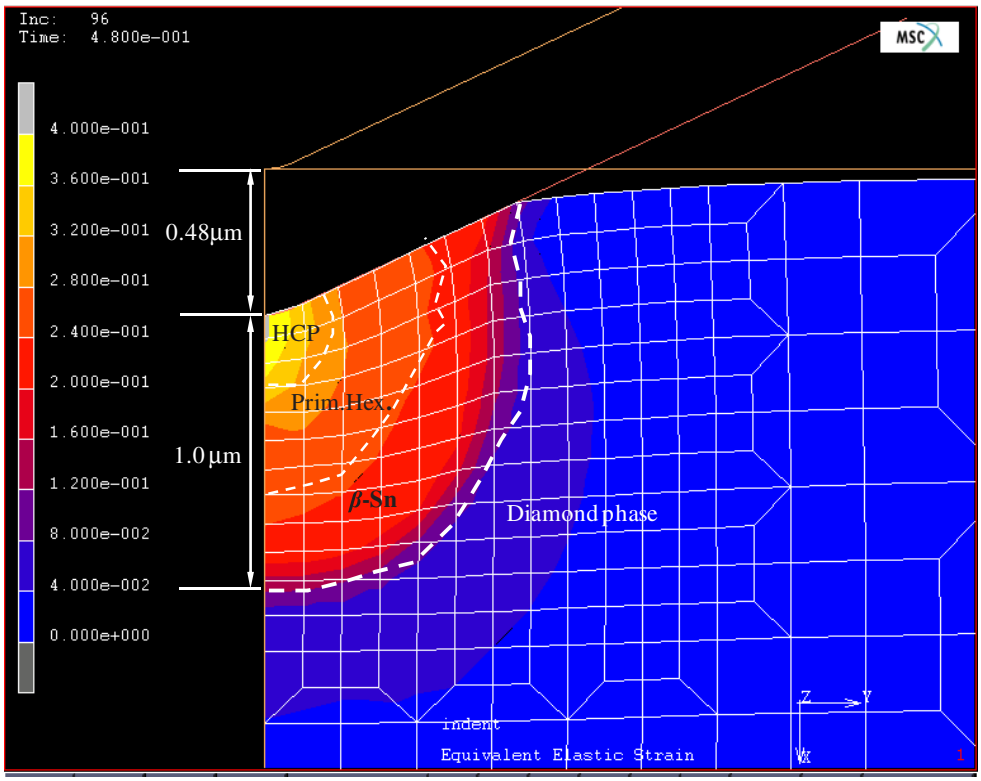

Figure 9. Simulated distribution of strain in silicon at a load of 50 mN.

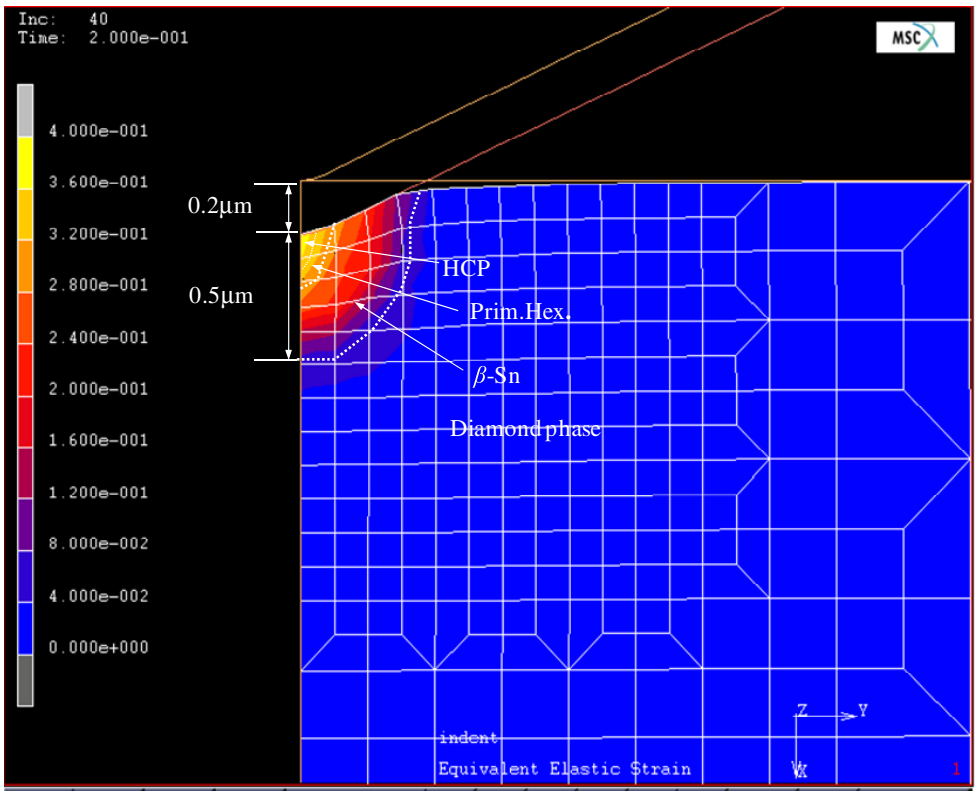

Figure 10. Simulated strain distribution in silicon at an indentation load of 10 mN.

from the indenter tip according to the strain gradient. In figure 9, the indentation depth is 0.48 μm, and the depth of the phase-transformation region measured from the indenter tip is 1.0 μm. Thus, we can say that the depth of the phase-transformation region is approximately twice the indentation depth.

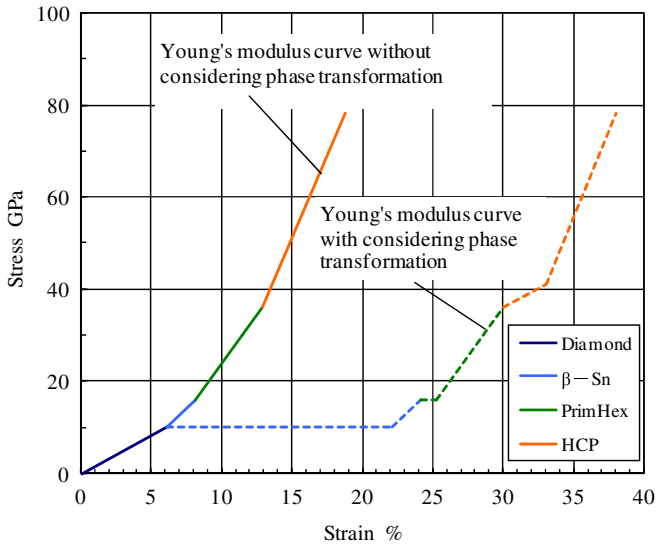

Figure 11. Stress–strain curves used for identifying the percentage of the phase-transformation-induced strain in the total indentation strain.

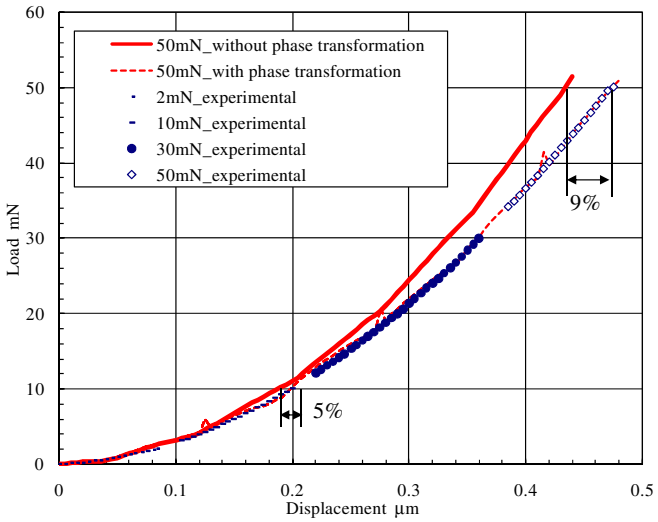

Figure 12. Comparison of simulated load–displacement curves with and without considering the equivalent Young's modulus of phase transformation.

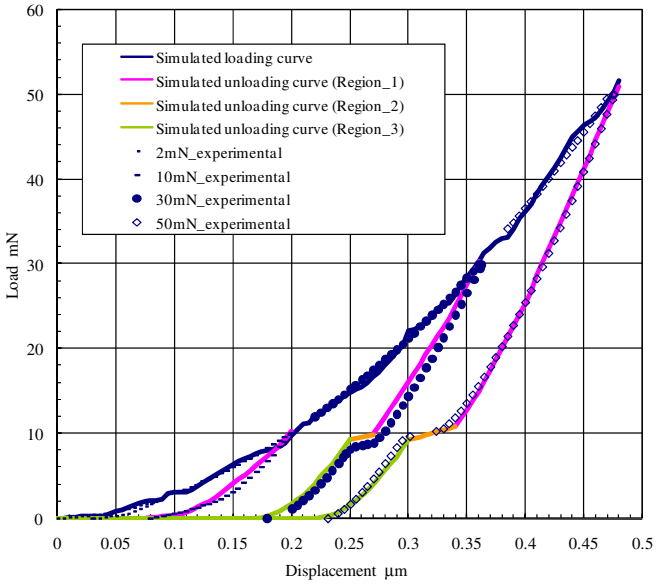

Figure 13. Comparison between the simulated load–displacement curves and the experimental results during unloading.

Figure 10 is a simulated strain distribution in silicon at a smaller indentation load of 10 mN. Although the load is only one-fifth of that in figure 9 (50 mN), the strain distribution is basically the same. That is, the high-pressure phases, namely, the HCP phase, the PrimHex phase and the β-Sn phase, are distributed concentrically from the center of the indenter tip to the outer region (diamond phase). From this result, it can be said that the indentation-induced phase-transformation mechanism during loading is independent of the indentation load. This fact is also supported by the experimental results in figure 2 where all the load–displacement curves under different loads follow the same trend in loading.

5.1.3. Strain relaxation due to phase transformation. As mentioned in section 1, we presume that there are two factors that cause stress relaxation during loading: the elastic deformation of each silicon phase, and the transformation among these phases. Next, to examine the respective percentages of these two factors in the total loading strain, FEM simulation was performed by considering Young's modulus of each silicon phase only and without considering the equivalent Young's modulus of phase transformation. The stress–strain curve for this simulation is shown in figure 11.

Figure 12 is a comparison of the simulated load–displacement curves with and without considering the equivalent Young's modulus of phase transformation. The experimental results of the load–displacement curves during loading are also shown in the figure. It can be seen that strain relaxation due to phase transformation increases as the indentation load increases. At a load of 10 mN, the strain due to phase transformation is approximately 5%; at a load of 50 mN, however, the strain increases to about 9%. From this fact, we can say that as the load increases, the loading energy has been increasingly absorbed by phase transformation and accumulated into the high-pressure phases. Moreover, because strain relaxation due to phase transformation from the diamond phase to the β-Sn phase is much more significant compared to other phase transformations (see figure 5), we can say that the loading energy has been mostly absorbed by phase transformation from the diamond phase to the β-Sn phase.

5.2. Results of the unloading process

5.2.1. Load–displacement curves. Using the stress–strain curves shown in section 4.2, the unloading process at various indentation loads was simulated. Figure 13 shows a comparison between the simulated load–displacement curves and the experimental results during unloading. The simulated curves were generally consistent with the experimental curves. From this fact, we can discuss the mechanical property of high-pressure silicon phases and the mechanism of phase transformation in unloading as follows.

In region 1 (before pop-out), all high-pressure phases, other than the β-Sn phase, will undergo reverse phase transformations during unloading, and all the phases will be unloaded at the same equivalent Young's modulus as that of the diamond phase ($E_{ave} = 163$ GPa). The reverse transformation from the β-Sn phase to the diamond phase does not occur, and instead, other non-equilibrium phases, such as amorphous phase and BC8 phase, will be generated. This is strongly supported by the fact that the electron diffraction pattern of the indented material after unloading shows a majority of amorphous phase dotted with the BC8 phase [17, 19]. This phase transformation also has the same equivalent Young's modulus as that of the diamond phase ($E_{ave} = 163$ GPa). The non-equilibrium phases generated by this non-irreversible phase transformation should be the dominant reason for residual strain after indentation. It should be mentioned that the indentation tests in the present work were performed at an unloading rate of 0.4–10 mN s^{-1}. At a much lower unloading rate, reverse phase transformation from the β-Sn phase to the diamond phase might occur.

As for region 2 (pop-out region), conventionally, pop-out has been considered as an effect of a sudden volume increase during the reverse phase transformations. However, in the present study, the simulation based on the equivalent Young's modulus of the reverse phase transformation could not generate pop-outs on the simulated load–displacement curves. Pop-outs occurred only when we used Young's modulus as small as 1/10 of that of the diamond phase. This fact indicates that pop-out might be a mechanical pinning phenomenon at the interface between the indenter and the silicon material. That is, as the indenter is withdrawn out of the indent, a kind of interaction force, which has been accumulated at the interface between the indenter and the silicon material, will be suddenly released. This interaction force might be related to an interfacial phenomenon, such as friction and slip–stick between the indenter and the silicon material, and is independent of the reverse phase transformations. The mechanism of pop-out events is in further investigation in our study.

In region 3, by using the same stress–strain relationship as that used in region 1, the simulation results agreed well with the experimental results. This fact indicated that the phase-transformation mechanism in unloading, before and after the pop-out, was the same. Inversely speaking, if there is no difference in the phase-transformation mechanism before and after the pop-out, then again we may say that pop-out is independent of phase transformation, and is a pure mechanical phenomenon at the interface between the indenter and the silicon material.

Next, we consider indentation tests at extremely small loads (2 mN, 10 mN) where no pop-out occurs. The simulated results were consistent with experimental results when we used the same stress–strain relationship as that of region 1 of a higher load (30 mN, 50 mN). Although the small load conditions (2 mN, 10 mN) correspond to region 3 (<10 mN) of the high load conditions (30 mN, 50 mN), silicon has been unloaded by Young's modulus of region 1 (>10 mN). This fact indicates that even at an extremely small load, the reverse phase transformation from the β-Sn phase to the non-equilibrium phases still occurs during unloading. However, in this case, strain accumulation in the indent is insufficient to cause a pop-out. From the above results, we may conclude that unloading is based on the same mechanism despite the fact that pop-out occurs or not. In other words, pop-out has no influence on the unloading mechanism.

5.2.2. Residual strain distribution. The changes in simulated residual strain distribution in the material around the indenter during unloading were investigated. Unloading was begun from the maximum load situation (50 mN) as has been shown in figure 9, where from the region beneath the indenter tip to the diamond phase, the HCP phase, the PrimHex phase and the β-Sn phase have been generated concentrically. Figure 14(*a*) is the strain distribution after unloading to the point just before the pop-out occurrence. Due to that the β-Sn phase cannot transform back to the diamond phase, residual strain in the form of non-equilibrium phases will be generated. The total volume of the β-Sn phase and the non-equilibrium phases is significantly larger than other high-pressure phases. The strain distribution at the end of pop-out is shown in figure 14(*b*), which is basically the same as that in figure 14(*a*). Finally, after silicon has been completely unloaded, all the high-pressure phases including the HCP phase, the PrimHex phase and the β-Sn phase have been changed into the non-equilibrium phases, as shown in figure 14(*c*). In figure 14(*a*)–(*c*), it is clear that the boundary between the non-equilibrium phases and the diamond phase does not change remarkably as the indentation load decreases. In other words, the non-equilibrium phase region expands gradually from its interface with the diamond phase toward the indenter tip during unloading.

In figure 14(*c*), the depth of the residual phase-transformation region is 1.0 μm, which is similar to the experimental result shown in the TEM image (see figure 3 of [19]), namely 0.75 μm. This fact strongly demonstrated the validity of the FE model and the silicon property factors used in this paper.

5.3. Summary of material properties in loading/unloading

The material properties, namely Young's modulus of each silicon phase and the equivalent Young's modulus of each phase transformation, used in the present study can be summarized as follows.

(1) *In loading*:

(A) The elastic modulus (in terms of average Young's modulus) increases with strain, namely, from the diamond phase to the HCP phase (diamond = 163 GPa, β-Sn = 304 GPa, PrimHex = 416 GPa, HCP = 790 GPa).

(B) The equivalent Young's modulus of each phase transformation is as small as 1/1000 of that of the diamond phase, except that of transformation from the PrimHex phase to the HCP phase, the literature of which under hydrostatic pressure is not available. In this work, we assigned it a value of 163 GPa, the same as that of the diamond phase.

(2) *In unloading*:

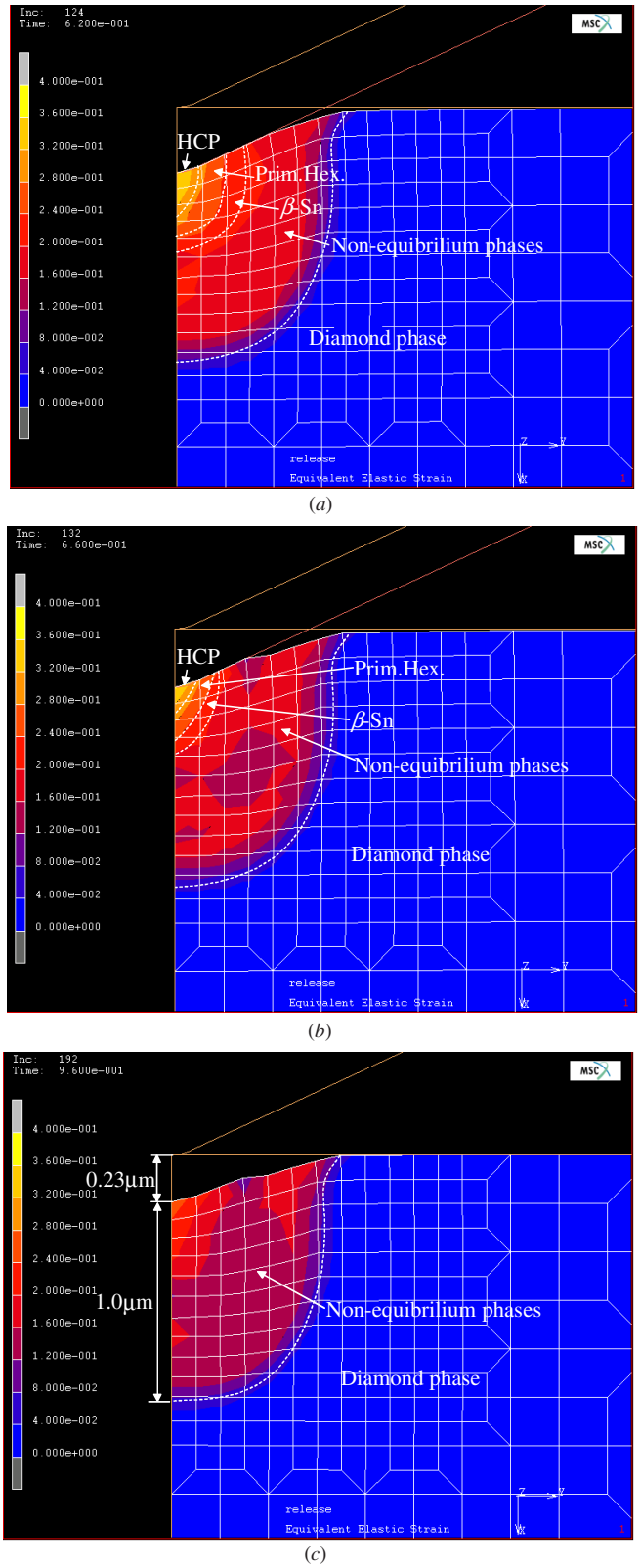

Figure 14. Strain distribution in silicon at different unloading stages: (*a*) before pop-out occurrence, (*b*) after pop-out and (*c*) after complete unloading.

(C) Before the occurrence of pop-out, Young's modulus of each silicon phase, namely, diamond, β-Sn, PrimHex and HCP, is the same as that of the loading process.

(D) Reverse phase transformations from HCP to PrimHex and from PrimHex to β-Sn have the same equivalent Young's modulus as those of loading, namely, $1/1000$ of that of the diamond phase. One exception is the reverse transformation from the β-Sn phase to the diamond phase, the equivalent Young's modulus of which is 163 GPa (the same as that of the diamond phase), different from that of loading. This is because transformation from the β-Sn phase to a non-equilibrium phase such as amorphous and BC8 phases has occurred.

(E) During pop-out, Young's modulus of all the silicon phases, except the diamond phase, is approximately $1/10$ of that of the diamond phase.

(F) Young's modulus of each silicon phase after pop-out is the same as that before pop-out occurrence, and also the same as that of small load conditions where no pop-out occurs.

6. Conclusions

Dynamic changes in stress/strain distribution and high-pressure phase distribution in the nanoindentation of single-crystal silicon have been simulated by FEM. The conclusions drawn from this study are as follows.

(1) By using the elastic property of each high-pressure phase and dealing with the high-pressure phase transformation as an equivalent elastic deformation, to which an equivalent Young's modulus is given, the simulated displacement–load curves during loading and unloading can be closely fitted to the experimental results.

(2) In loading, the distribution pattern of high-pressure phases beneath the indenter is independent of the load. The depth of the phase-transformation region measured from the indenter tip is approximately twice the indentation depth.

(3) As the indentation load increases, loading energy is increasingly absorbed by phase transformation (mostly by the phase transformation from the diamond phase to the β-Sn phase) and accumulated as the elastic strain energy of the high-pressure phases.

(4) In unloading, all high-pressure phases other than the β-Sn phase will perform reverse phase transformations with an equivalent Young's modulus approximately the same as that of loading. The β-Sn phase does not transform back to the diamond phase but to other non-equilibrium phases at an equivalent Young's modulus approximately the same as that of the diamond phase. This is the dominant reason for residual strain in silicon nanoindentation.

(5) During unloading, the non-equilibrium phase expands from its interface with the surrounding diamond phase toward the indenter tip, but the boundary between the non-equilibrium phases and the diamond phase does not change with the load.

(6) Unloading is based on the same mechanism despite the maximum indentation load and despite the presence/absence of pop-outs. Pop-out might be a pure interfacial phenomenon between the diamond indenter and the silicon material.

Appendix

A.1. Atomic density of diamond-phase silicon

If we assume the atomic density of diamond-phase silicon as d (unit: g cm^{-3}), then d can be described as

$$d = \frac{W}{V} \tag{A.1}$$

where W is the weight of the atoms in a unit cell (unit: g), and V is the volume of a unit cell (unit: cm^3). In equation (A.1), W can be expressed as

$$W = \frac{M}{N} \cdot n \tag{A.2}$$

where M is the atomic weight of silicon (28.086 g mol^{-1}), N is the Avogadro number (6.023×10^{23} mol^{-1}) and n is the number of atoms in a unit cell ($n = 8$ according to table 2). We also know from table 2 that the lattice constant of diamond-phase silicon is $a = 5.431 \times 10^{-8}$ cm so that the volume of a unit cell is $V = a^3 = 1.6019 \times 10^{-22}$ cm^3. As a result, we can obtain the atomic density of diamond-phase silicon as $d = 2.329$ g cm^{-3}.

A.2. Atomic density of amorphous silicon

From previous cross-sectional TEM observations of silicon indents [19], we have found that the residual non-equilibrium phase of silicon after indentation is mainly amorphous, slightly dotted with a few microcrystalline (BC8) grains. In this section, to estimate the atomic density of amorphous silicon, we disregard the microcrystalline phase. If we suppose that the volume of amorphous silicon beneath the indent is V_a and the volume of the residual indent is V_b, then the volume ratio (R) of amorphous silicon to initial diamond-phase silicon can be expressed as

$$R = \frac{V_a}{V_a + V_b}. \tag{A.3}$$

From the TEM image of silicon indents in figure 3 of [19], we obtained $R = 0.819$. According to the law of conservation of mass before and after indentation, the atomic density of amorphous silicon can be obtained as

$$d_a = \frac{d}{R} \tag{A.4}$$

where d is the atomic density of diamond-phase silicon. Since $d = 2.329$ g cm^{-3}, the atomic density of amorphous silicon is $d_a = 2.844$ g cm^{-3}.

References

[1] Blake P N and Scattergood R O 1990 Ductile regime machining of germanium and silicon *J. Am. Ceram. Soc.* **73** 949–57

[2] Shibata T, Ono A, Kurihara K, Makino E and Ikeda M 1994 Cross-section transmission electron microscope observations of diamond-turned single-crystal Si surfaces *Appl. Phys. Lett.* **65** 2553–5

[3] Puttick K E, Whitmore L C, Chao C L and Gee A E 1994 Transmission electron microscopy of nanomachined silicon crystals *Phil. Mag.* A **69** 91–103

[4] Jeynes C, Puttick K E, Whitmore L C, Gartner K, Gee A E, Millen D K, Webb R P, Peel R M A and Sealy B J 1996 Laterally resolved crystalline damage in single-point-diamond-turned silicon *Nucl. Instrum. Methods Phys. Res.* B **118** 431–6

[5] Yan J, Yoshino M, Kuriyagawa T, Shirakashi T, Syoji K and Komanduri R 2001 On the ductile machining of silicon for micro electro-mechanical systems (MEMS), opto-electronic and optical applications *Mater. Sci. Eng.* A **297** 230–4

[6] Yan J, Syoji K, Kuriyagawa T and Suzuki H 2002 Ductile regime turning at large tool feed *J. Mater. Process. Technol.* **121** 363–72

[7] Yan J, Takahashi H, Tamaki J, Gai X and Kuriyagawa T 2005 Transmission electron microscopic observation of nanoindentations made on ductile-machined silicon wafers *Appl. Phys. Lett.* **87** 211901

[8] Gridneva I V, Milman Y V and Trefilov V I 1972 Phase transition in diamond-structure crystals during hardness measurements *Phys. Status Solidi* a **14** 177–82

[9] Eremenko V G and Nikitenko V I 1972 Electron microscope investigation of the microplastic deformation mechanism of silicon by indentation *Phys. Status Solidi* a **14** 317–30

[10] Clarke D R, Kroll M C, Kirchner P D and Cook R F 1988 Amorphization and conductivity of silicon and germanium induced by indentation *Phys. Rev. Lett.* **60** 2156–9

[11] Pharr G M, Oliver W C and Harding D S 1991 New evidence for a pressure-induced phase transformation during the indentation of silicon *J. Mater. Res.* **6** 1129–30

[12] Callahan D L and Morris J C 1992 The extent of phase transformation in silicon hardness indentations *J. Mater. Res.* **7** 1614–7

[13] Kailer A, Gogotsi Y G and Nickel K G 1997 Phase transformations of silicon caused by contact loading *J. Appl. Phys.* **81** 3057–63

[14] Bradby J E, Williams J S, Wong-Leung J, Swain M V and Munroe P 2000 Transmission electron microscopy observation of deformation microstructure under spherical indentation in silicon *Appl. Phys. Lett.* **77** 3749–51

[15] Zarudi I and Zhang L C 1999 Structure changes in mono-crystalline silicon subjected to indentation—experimental findings *Tribol. Int.* **32** 701–12

[16] Saka H, Shimatani A, Sugamura M and Suprijadi 2002 Transmission electron microscopy of amorphization and phase transition beneath indents in Si *Phil. Mag.* A **82** 1971–81

[17] Zarudi I, Zou J and Zhang L C 2003 Microstructures of phases in indented silicon: a high resolution characterization *Appl. Phys. Lett.* **82** 874–6

[18] Jang J, Lance M J, Wen S, Tsui T Y and Pharr G M 2005 Indentation-induced phase transformations in silicon: influences of load, rate and indenter angle on the transformation behavior *Acta Mater.* **53** 1759–70

[19] Yan J, Takahashi H, Gai X, Harada H, Tamaki J and Kuriyagawa T 2006 Load effects on the phase transformation of single-crystal silicon during nanoindentation tests *Mater. Sci. Eng.* A **423** 19–23

[20] Yoshino M, Aoki T, Chacrasekaran N, Shirakashi T and Komanduri R 2001 Finite element simulation of plane strain plastic–elastic indentation on single-crystal silicon *Int. J. Mech. Sci.* **43** 313–33

[21] Hebbache M and Zemzemi M 2003 Nanoindentation of silicon and structural transformation: three-dimensional contact theory *Phys. Rev.* B **67** 233302

[22] Vodenitcharova T and Zhang L C 2003 A mechanics prediction of the behaviour of mono-crystalline silicon under nano-indentation *Int. J. Solids Struct.* **40** 2989–98

[23] Hu J Z and Spain I L 1984 Phases of silicon at high pressure *Solid State Commun.* **51** 263–6

[24] Jamieson J C 1963 Crystal structures at high pressures of metallic modifications of silicon and germanium *Science* **139** 762–4
[25] McMahon M J and Nelmes R J 1993 *Phys. Rev.* B **47** 8337
[26] Hu J Z, Merkle L D, Menoni C S and Spain I L 1986 Crystal data for high-pressure phases of silicon *Phys. Rev.* B **34** 4679–84
[27] Olijnyk H, Sikka S K and Holzapfel W B 1984 Structural phase transition in Si and Ge under pressure up to 50 GPa *Phys. Lett.* A **103** 137–40
[28] Duclos S J, Vohra Y K and Ruoff A L 1990 Experimental study of the crystal stability and equation of state of Si to 248 GPa *Phys. Rev.* B **41** 12021–8
[29] Duclos S J, Vohra Y K and Ruoff A L 1987 Hcp-to-fcc transition in silicon at 78 GPa and studies to 100 GPa *Phys. Rev. Lett.* **58** 775–7
[30] Kasper J S and Richard S M 1964 The crystal structures of new forms of silicon and germanium *Acta Crystallogr.* **77** 752–5
[31] Piltz R O, Maclean J R, Clark S J, Ackland G J, Hatton P D and Crain J 1995 Structure and properties of silicon XII: a complex tetrahedrally bonded phase *Phys. Rev.* B **52** 4072–85
[32] Yin M T 1984 Si-III (BC-8) crystal phase of Si and C; structural properties, phase stabilities, and phase transitions *Phys. Rev.* B **30** 1773–6